The role of pre-existing discontinuities in the development of extensional faults: An analog modeling perspective

Lorenzo Bonini [a, c, *], Roberto Basili [b], Giovanni Toscani [c], Pierfrancesco Burrato [b], Silvio Seno [c], Gianluca Valensise [b]

[a] Dipartimento di Matematica e Geoscienze, Università di Trieste, Trieste, Italy
[b] Istituto Nazionale di Geofisica e Vulcanologia, Rome, Italy
[c] Dipartimento di Scienze della Terra e dell'Ambiente, Università di Pavia, Italy

ARTICLE INFO

Accepted 5 March 2015

Keywords:
Extension
Normal fault
Pre-existing fault
Analogue modeling
Blind fault
Active tectonics

ABSTRACT

Several mountainous regions are currently affected by syn- or post-orogenic active extension. We investigate how a newly-formed normal fault interacts with structures inherited from a previous contractional phase. To this end, we use analog models that adopt an innovative technique for performing a precut that mimics such inherited structures into a clay layer; this clay layer is laid on top of a master fault simulated by two rigid blocks sliding along an inclined plane. We carry out six experiments with variously oriented precuts and compare the results with those obtained in a reference isotropic experiment. All other conditions are identical for all seven realizations. Fault evolution is monitored by taking closely-spaced snapshots analyzed through the Digital Image Correlation method. We find that the upward propagation of the normal fault can be either accelerated or decelerated depending on the presence of a precut and its orientation. Such precuts can also promote or inhibit the formation of bending-moment faults. These interactions between master fault and precut also affect the shape of the fault-related syncline–anticline pair.

1. Introduction

Long-term geological processes, such as the growth and development of extensional faults from their embryonic stage (blind faults) to a mature stage (basin-bounding faults), cannot be appreciated on a human timescale. Two fundamental options exist to overcome this limitation. One is the analysis of natural faults at different stages of maturity at different locations; the other is the analysis of faults through modeling. In principle, the first strategy should be preferred, but identifying a suite of faults having different age and sharing a similar tectonic framework may turn out to be extremely difficult. The second strategy is easier to pursue but its assumptions and limitations need to be carefully considered. Conceptual evolutionary models predict that in a uniform material faults form through the coalescence of Mode I fractures subsequently reactivated in shear (e.g. Segall and Pollard, 1983; Martel et al., 1988; Pollard and Aydin, 1988; Mandl, 2000; Scholz, 2002; Gudmundsson, 2011). The growth history of a natural extensional fault, however, is often more complex than one might expect from such simple models. Rock variability and the presence of older structures (e.g., pre-existing faults) may play a crucial role, for instance, in affecting the geometry of the fault and its extent. These occurrences are nearly inevitable when extension takes place in mountain belts where syn- or post-orogenic extensional structures develop in complex settings created by the superposition of different rock types separated by thrust faults (Fig. 1). Several major mountain belts are currently undergoing extension, including the Himalayas (Molnar et al., 1993), the Andes (Dalmayrac, and Molnar, 1981), the Basin and Range (Wernicke, 1981; Malavieille, 1993), the Taiwan Orogen (Teng, 1996), the Alps (Selverstone, 1988; Bonini et al., 2010; Maino et al., 2013), the Apennines (Elter et al., 1975; Hyppolite et al., 1994; Tavarnelli et al., 2001, 2003), and the Pyrenees (Chevrot et al., 2011; Lacan and Ortuño, 2012). The growth of faults in these heterogeneous layered settings has been the object of a number of studies (see van Gent et al., 2010; Roche et al., 2013 and references therein). A few studies have also discussed how faults develop when interacting with pre-existing mechanical weaknesses, such as inherited fault zones or thin weak rock layers

* Corresponding author. Dipartimento di Matematica e Geoscienze, Università di Trieste, Trieste, Italy.
E-mail address: lbonini@units.it (L. Bonini).

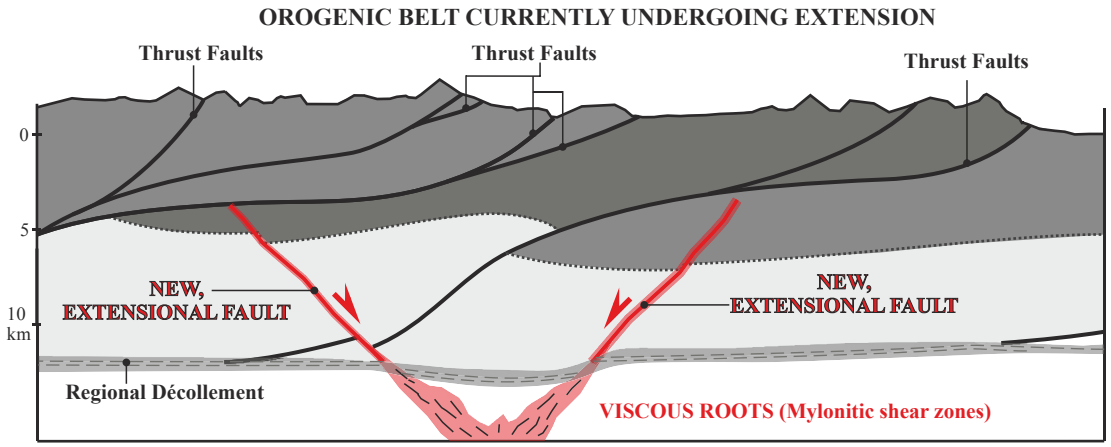

Fig. 1. Schematic cross section showing the early blind phase of an extensional system where new faults grow up and interact with inherited mechanical discontinuities such as thrust faults.

(e.g., Williams et al., 1989; Faccenna et al., 1995; Tavarnelli et al., 1996a, 1996b; Cosgrove and Ameen, 2000; Withjack and Callaway, 2000; Tavarnelli et al., 2001; Tvedt et al., 2013; Di Domenica et al., 2014; Tong et al., 2014). In addition, theoretical and numerical analyses have shown that even thin mechanical weaknesses may deflect, stop, decelerate or accelerate the propagation of new faults (e.g., Cooke and Pollard, 1997; Roering et al., 1997; Mandl, 2000).

In this study we investigate how the growth of an extensional fault is affected by the presence of a pre-existing frictional discontinuity located in the rock volume overlying the fault itself. To this end we performed analog modeling through a series of six experiments using a clay layer; in each realization a precut is placed with variable orientation with respect to a master fault, thus simulating simple but different inherited structural settings. The results of these experiments are compared with the state of deformation of a reference isotropic experiment (no precut above the fault). We quantify the strain-rate distribution inside the different experiments and reconstruct the evolution of any fault-related folds at significant steps.

Our results indicate that during the evolution of a growing extensional fault any pre-existing discontinuity affects (i) the propagation rate of new faults and their ability to reach the surface, (ii) the development of secondary brittle structures related to fault-propagation folding, and (iii) the shape of the related accommodation space together with the migration of the syncline hinge through time. We claim that these elements can be related to the presence and orientation of pre-existing mechanical discontinuities in natural cases.

2. Method and experimental setup

Two analog materials are commonly used to investigate the evolution of extensional structures: dry sand and wet clay. These two materials have different properties and are selected by modelers based on the goal to be pursued (Eisenstadt and Sims, 2005). Dry sand is classically used to analyze broad deformation zones and fault kinematics (e.g. Davis et al., 1983; McClay and Bonora, 2001; Ahmad et al., 2014; Toscani et al., 2014; Philippon et al., 2015), as well as the brittle surface expression of blind faults (e.g. Bonini et al., 2011; Galuppo et al., 2015). Wet clay is especially used in studies devoted to analyzing the development of faults and fractures (e.g. Cloos, 1968; Withjack and Jamison, 1986), and the potential reactivation of pre-existing faults (e.g. Eisenstadt and Sims, 2005; Bonini et al., 2014).

In this study we use wet clay to simulate the deformation patterns associated with an extensional, initially blind, master fault (Fig. 2). As regards the clay type, we adopt wet kaolin because it is one of the most used and tested clay types for simulating faulting and folding in brittle crustal rocks (e.g., Withjack et al., 1990; Eisenstadt and Sims, 2005; Miller and Mitra, 2011; Cooke and van der Elst, 2012).

The experimental apparatus is composed by two rigid blocks juxtaposed along 45° sloping sides, which represent the plane of the master fault. We adopted a dip of 45° for the master fault because worldwide compilations of normal faults show that this is the most common value in tectonically active regions (Jackson and White, 1989; Collettini and Sibson, 2001).

Wet clay covers the two rigid blocks and represents rocks located above the master fault (Fig. 2). The footwall block is fixed, whereas the hanging wall block is allowed to slide downward along the sloping side. The displacement of the moving block is controlled by a stepper-motor at a constant velocity of 0.005 mm/s. The clay is wet kaolin with density of 1.65 g/cm^3, water content of 60% by mass, shear strength in the range 50–120 Pa (Eisenstadt and Sims, 2005; Cooke and van der Elst, 2012), and friction coefficient equal to 0.6. Using well established scaling rules (e.g., Hubbert, 1937) we assume that under these experimental conditions 1 cm in our experiment corresponds to about 1 km in nature. In all the experiments the clay layer is 5 cm-thick, thus representing a 5 km-thick brittle continental crust in nature. Black quartz sand grains are placed on the model side to act as displacement markers by creating a visual contrast with the pale-colored clay, hence allowing the model evolution to be monitored. In addition to mapping brittle structural features such as newly-formed fractures and faults, this technique allows us to identify peculiar features of the displacement field, including the trishear zone (Hardy and Ford, 1997; Allmendinger, 1998), and to obtain a high-resolution quantification of the deformation taking place during the experiments. Fault evolution, displacement field, and strain-rate distribution are investigated through the Digital Image Correlation method (D.I.C.; Pan et al., 2009) by analyzing side photographs taken at every 0.5 mm of displacement on the master fault using the PIVlab software (Garcia, 2011; Thielicke, 2014; Thielicke and Stamhuis, 2014).

What makes wet kaolin especially suitable for our purposes is the possibility of precutting the clay layer to introduce thin

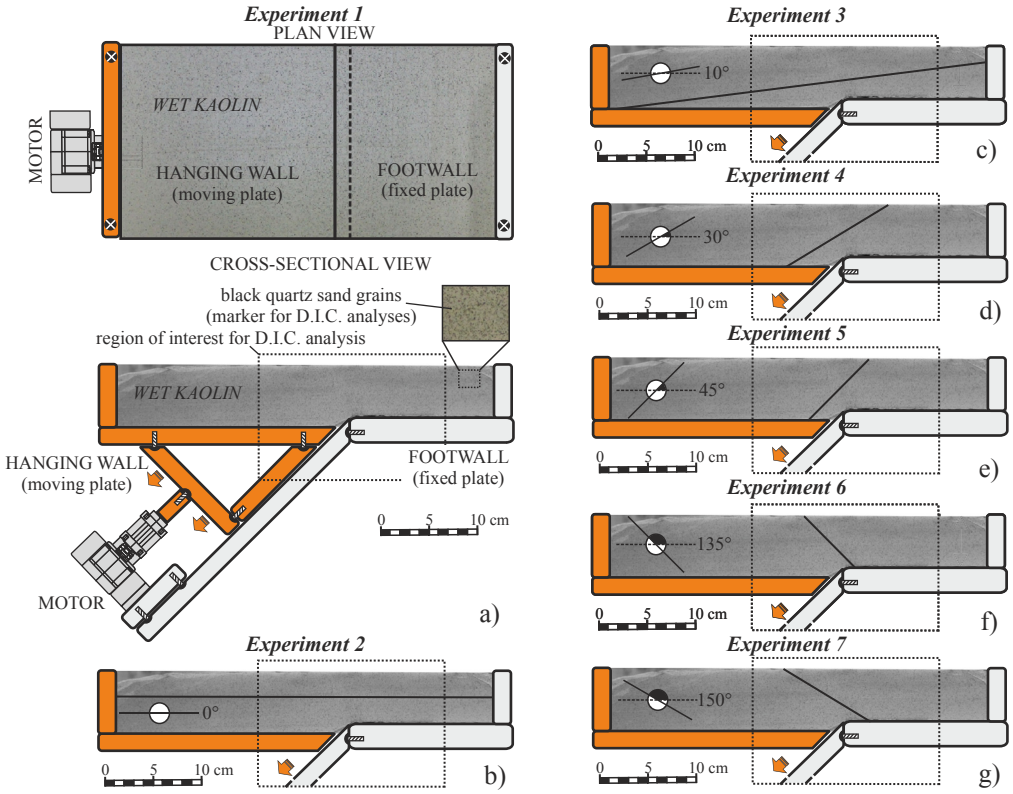

Fig. 2. a) Plan and side views of the apparatus and initial setup of the isotropic experiment E1. **b-g)** Initial setups for the precut experiments E2-E7 (the precut is shown by a black, thick line on the side of the clay layer).

mechanical discontinuities that simulate pre-existing faults or thin layers of weaker rocks. The precut is ~200 μm thick and is obtained by sliding an electrified blade into the clay layer before starting the deformation process. This technique has already been applied to reproduce long-lived faults both in strike-slip systems (Cooke et al., 2013) and in extensional regimes (Paul and Mitra, 2013; Bonini et al., 2014).

Using this setup we conduct seven experiments named from E1 through E7 (Fig. 2a–h, Table 1). E1 is a mechanically isotropic experiment (i.e. without precut). E2 has a horizontal precut in the middle of the clay layer. E3, E4 and E5 have precuts dipping 10°, 30°, and 45°, respectively, with the same dip direction of the master fault (i.e., synthetic planes). The last two experiments, E6 and E7, have a precut dipping 45° and 30°, respectively, both with opposite dip direction with respect to the master fault (i.e. antithetic planes).

The precut is spatially arranged such that it consistently runs 2.5 cm above the tip of the master fault for all experiments. For simplicity, we show snapshots taken at the end of regular intervals of 0.5 cm of displacement on the master fault. In the following, each interval is denoted as follows: 0.0–0.5 cm, Early Stage; 0.5–1.0 cm, Middle Stage; 1.0–1.5 cm, Late Stage. For each stage we provide a display of fault and fracture traces, a set of displacement vectors, and the strain-rate distribution within the clay layer.

3. Experimental results

3.1. Experiment E1: isotropic

During the Early Stage a newly-formed synthetic fault and a smaller antithetic fault propagate upward from the upper tip of the master fault (Fig. 3a), and the fault-propagation folding produces a gentle monocline. The displacement field indicates a trishear zone located above the tip of the master fault (Fig. 3b), and the strain

Table 1
Summary of initial conditions and results of each experiment.

	Initial conditions			Results					
	Precut	Dip angle	Dip direction	Propagation rate[a]			Antithetic faults created	Shallow brittle structures created	Syncline hinge migration rate[a]
				Below precut	Across precut	Above precut			
E1	No	–	–	–	–	–	Yes	Yes	–
E2	Yes	Horizontal	–	≈	>	>>	No	Yes	≈
E3	Yes	10°	Synthetic	≈	>	<<	Yes	Yes	≈
E4	Yes	30°	Synthetic	≈	R	R	Yes	No	<
E5	Yes	45°	Synthetic	≈	R	R	Yes	No	–
E6	Yes	45°	Antithetic	≈	>	<	Yes	Yes	<
E7	Yes	30°	Antithetic	≈	>	<	Yes	Yes	<<

[a] Mathematical symbols represent relative values of propagation and syncline hinge migration rates with respect to the isotropic experiment (E1); letter "R" stands for precut reactivation.

analysis shows that most of the deformation is related to the upward-propagating synthetic fault (Fig. 3c).

In the Middle Stage the first synthetic fault slightly propagates upward (Fig. 3d) and two branches appear on both sides of it. Such faults grow by connecting previously-formed small cracks. At the free surface, the steepening of the monocline produces two downward-propagating faults (bending-moment faults).

During the Late Stage upward- and downward-propagating faults connect to each other, thereby forming a continuous fault plane that extends from the tip of the rigid hanging wall block up to the free surface (Fig. 3g), and there it forms a fault free face. Displacement vectors confirm the decoupling between the two sides of the fault in the clay layer, showing no motion of the footwall (Fig. 3h). Overall the strain-rate distribution shows that most of the deformation is concentrated along the main synthetic fault, though a secondary synthetic structure located in its hanging wall displays significant activity (Fig. 3i). The heterogeneous strain-rate distribution along the fault traces suggests that these faults form by linking small cracks.

In summary, the isotropic model shows that after about 1.5 cm of displacement imparted to the rigid blocks the fault has propagated enough to reach the free surface. This value is then used as a reference maximum displacement to compare the results obtained from the other experiments at the same step. In case the propagating fault reaches the surface before this reference maximum displacement, the experiment is stopped.

3.2. Experiment E2: horizontal precut

In the Early Stage a newly-formed, synthetic fault propagates upward and intersects the horizontal precut (Fig. 4); a small fracture is located above its upper tip, and a bending-moment fault at the free surface accommodates the development of the monocline (Fig. 4a). Displacement vectors depict a trishear zone whose apical angle is located close to the precut (Fig. 4b), attesting faster upward fault propagation than in E1 (compare with Fig. 3b). The strain-rate distribution shows that most of the deformation is confined below the precut (Fig. 4c).

As the experiment proceeds to the Middle Stage the upward-propagating fault crosses the precut and connects with overlying fractures and with a newly-formed downward-propagating fault. This new fault system cuts the entire clay layer, as testified by the absence of displacement in its footwall (Fig. 4d). The experiment is thus stopped at the end of this stage. The fault-related folding at this stage produces bending-moment faults at the free surface. The strain-rate distribution shows that most of the slip falls along fault segments that formed in the Early Stage (Fig. 4e).

3.3. Experiment E3: synthetic, 10° dipping precut

During the Early Stage a new fault forms and propagates upward at a slower rate than that of E2, yet faster than the homologous fault in E1 (Fig. 5a). Unlike the first two experiments, no brittle structures are seen above the precut. The displacement field shows a trishear zone that crosses the precut (Fig. 5b). The vectors within the trishear zone exhibit a larger horizontal component than in E1 and E2. The strain analysis shows only diffuse deformation above the precut (Fig. 5c).

In the Middle Stage the upward-propagating fault reaches the discontinuity and stops (Fig. 5d, f); only few secondary fractures form at its tip without significant shearing. Two antithetic faults forms in the hanging wall of the master fault and a new bending-moments fault accommodates extension at the free surface. The

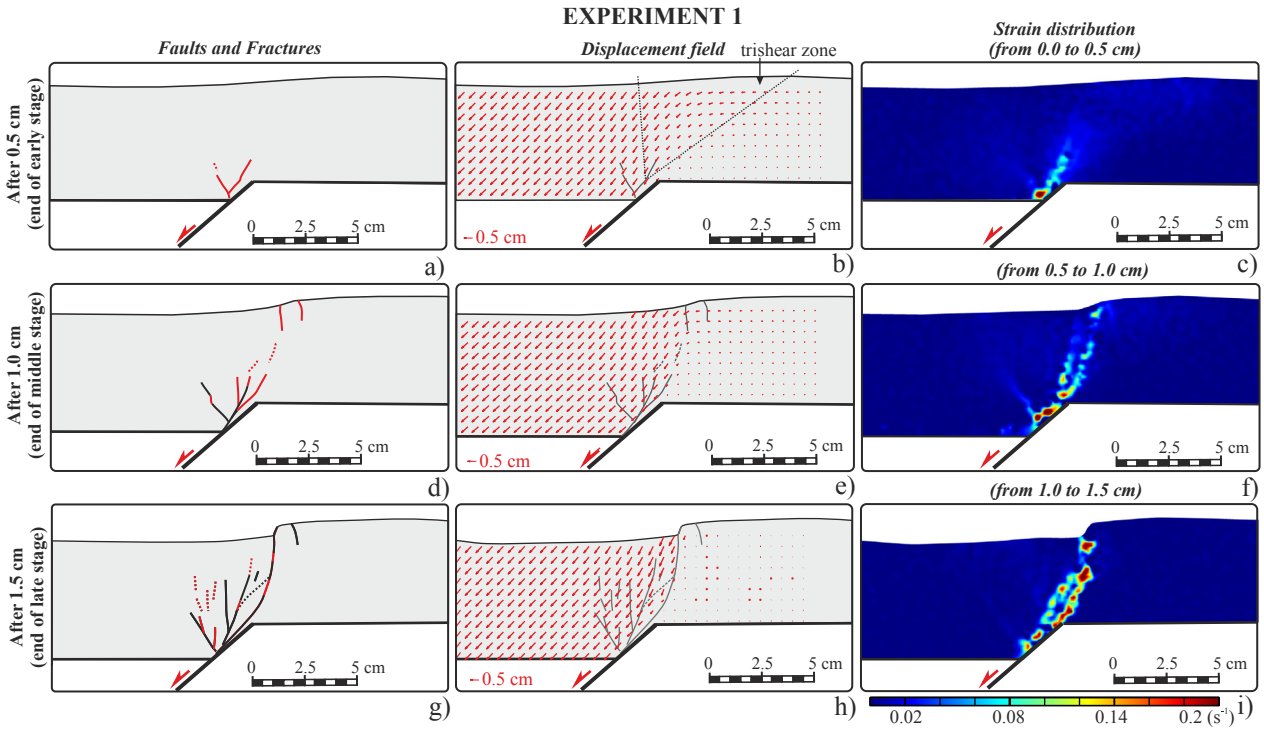

Fig. 3. Side view of the isotropic experiment E1 after 0.5, 1.0 and 1.5 cm of displacement on the master fault (end of early, middle, and late stages, respectively). The fault traces in the left-hand panels (**a, d, g**) were detected through visual inspection: the red lines marks the newly-formed faults developed in the specified stage; black lines are faults formed during previous stages. Central panels (**b, e, h**) show the displacement field detected using D.I.C. (red arrows) and the boundaries of the trishear zone (dotted lines), when present. Right-hand panels (**c, f, i**) display the strain-rate distribution. (For interpretation of the references to colour in this figure legend, the reader is referred to the web version of this article.)

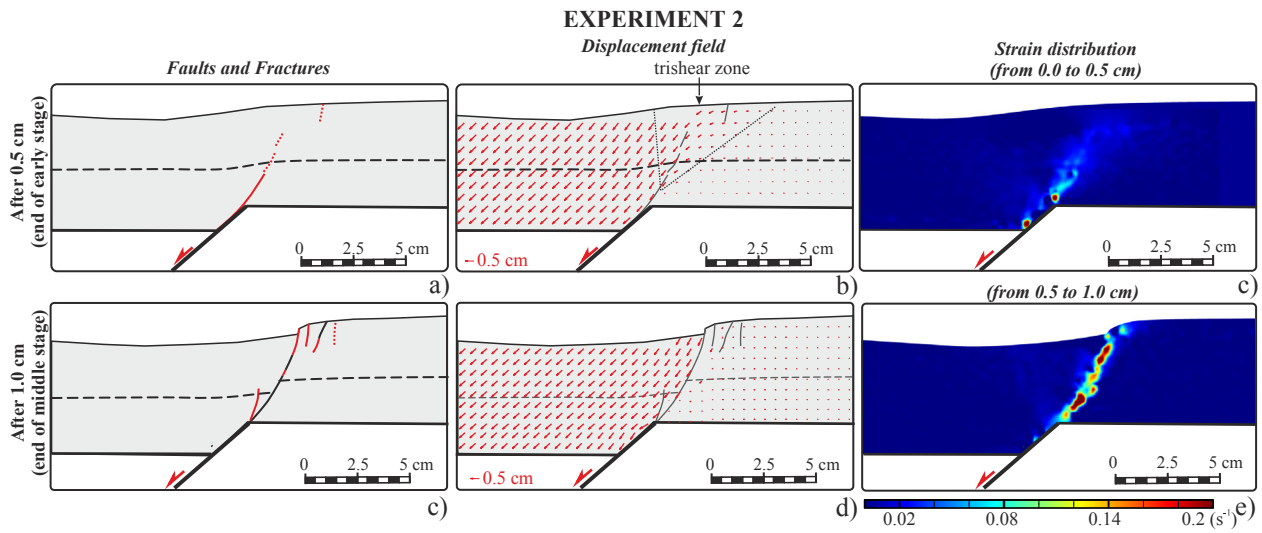

Fig. 4. Side view of E2 (horizontal precut). The dashed lines mark the precut; other symbols as in Fig. 3.

strain analysis shows that most of the deformation is confined below the precut (Fig. 5f).

In the Late Stage the upper tip of the upward-propagating fault remains in the vicinity of the precut (Fig. 5g). Brittle deformation is accommodated in its footwall by another small fracture located close to the precut and by bending-moment faults. The strain-rate distribution and displacement vectors show that there is no connection between upward- and downward-propagating structures. Therefore, at the final step of this experiment the slip at depth is not transferred all the way to the free surface.

3.4. Experiment E4: synthetic, 30° dipping precut

During the Early Stage a new fault forms at tip of the master fault and by propagating upward quickly reaches the precut (Fig. 6a). Both the displacement field and the strain-rate distribution show that the upper part of the precut has been slightly reactivated. The composite structure that includes the newly-formed fault and the reactivated precut inhibits the formation of a trishear zone, leaving the footwall almost undeformed (Fig. 6b, c). In the Middle Stage a new synthetic fault forms in the footwall of

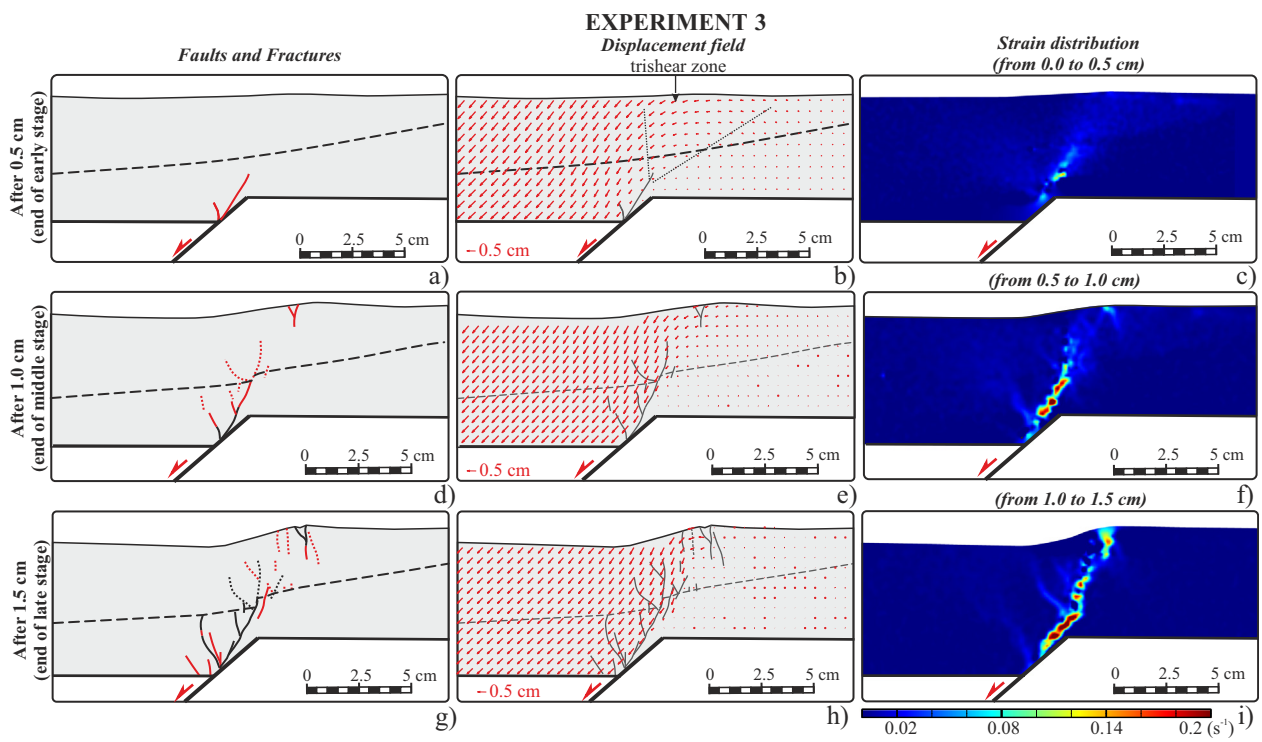

Fig. 5. Side view of E3 (synthetic, 10° dipping precut). The dashed lines mark the precut; other symbols as in Fig. 3.

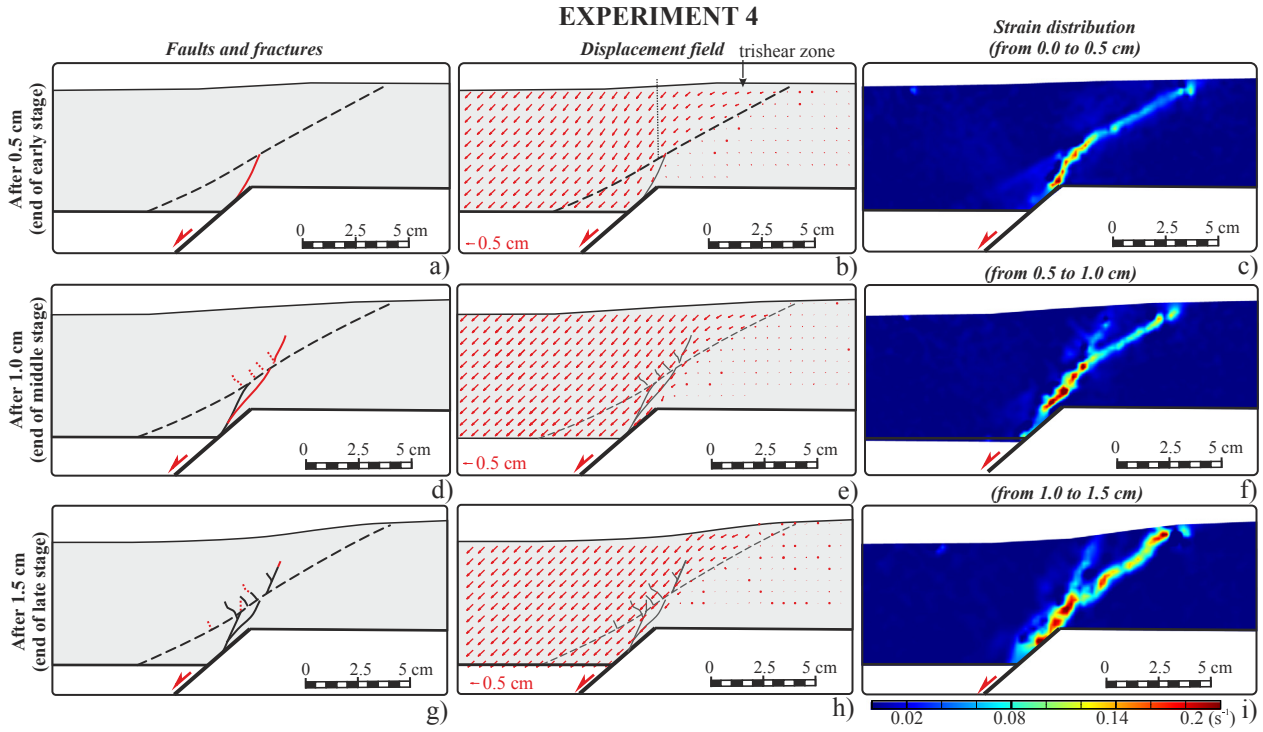

Fig. 6. Side view of E4 (synthetic, 30° dipping precut). The dashed lines mark the precut; other symbols as in Fig. 3.

the previously formed fault (Fig. 6d) and slip on the precut increases (Fig. 6e, f). Small fractures form in the zone where newly-formed faults meet the reactivated section of the precut. These fractures appear to be related to the flexure of the hanging-wall block due to the sliding along the composite structure. In the Late Stage (Fig. 6g) the displacement vectors and the strain-rate distribution show that this composite structure reaches a mature stage and the displacement of the rigid blocks is transferred up to the free surface through the precut (Fig. 6h, i). A secondary synthetic fault located in the hanging wall of the composite structure propagates a bit farther upward, yet it does not reach the free surface. Unlike previous experiments (E1, E2, E3), no bending-moments faults are formed at the free surface.

3.5. Experiment E5: synthetic, 45° dipping precut

In the Early Stage an upward-propagating fault reaches the precut, forming a composite fault that immediately transfers the displacement all the way to the free surface (Fig. 7). Both the displacement field and strain-rate distribution (Fig. 7b, c) show that slip is rather uniformly distributed along the precut. The experiment is then stopped.

3.6. Experiment E6: antithetic, 45° dipping precut

During the Early Stage a new fault develops from the tip of the master fault (Fig. 8); its propagation produces a somehow irregular trishear zone above it (Fig. 8b). The strain-rate distribution shows a partial reactivation of the precut, especially in the section near the newly formed fault (Fig. 8c). In the Middle Stage the upward-propagating fault reaches the precut and stops (Fig. 8d). Meanwhile, small fractures form in the hanging wall of the precut, some due to bending. Near the free surface the horizontal component of displacement dominates, thereby promoting the formation of bending-moment faults that are more evident in this experiment than in all other experiments (Fig. 8e). The strain-rate distribution shows that much of the deformation is localized on the surface faults (Fig. 8f). During the Late Stage (Fig. 8g) the upward-propagating fault splits into two splays and crosses the precut. Bending-moment faults are well-developed and exhibit a sizable vertical displacement; yet they do not show a direct connection with the upward-propagating faults (Fig. 8h). The strain-rate distribution shows the reactivation of the precut (Fig. 8i).

3.7. Experiment E7: antithetic, 30° dipping precut

In the Early Stage (Fig. 9) the upward-propagating fault is slightly more developed and the displacement field is less irregular than in E6 (Figs. 9b and 8b). The strain-rate distribution shows only a modest reactivation along the precut and most of the strain is concentrated along newly-formed faults (Fig. 9c). During the Middle Stage the upward-propagating fault reaches the precut and bending-moment faults start propagating downward from the free surface (Fig. 9d, e). In this stage the strain-rate distribution shows that the precut is not reactivated and part of the deformation focuses along an embryonic antithetic fault (Fig. 9f). In the Late Stage upward- and downward-propagating faults are almost connected (Fig. 9g), as testified by the displacement vectors and by the strain-rate distribution (Fig. 9h, i). Similarly to E6, also in this experiment bending-moment faults exhibit a considerable vertical offset, but in this case also the newly-formed antithetic fault produces significant offset of the free surface.

4. Discussion

In all experiments with precuts (E2-7), and starting from the very early development stage, the geometry and kinematics of brittle structures, the shape of the related folds, the displacement fields, and the strain-rate distributions differ from those seen

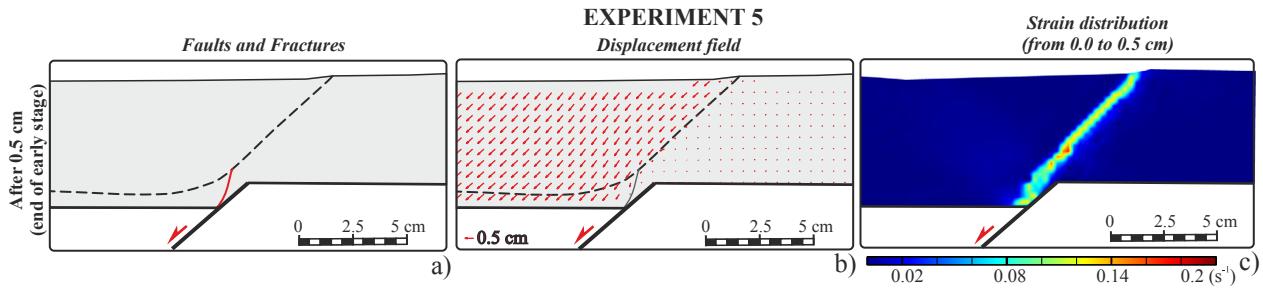

Fig. 7. Side view of E5 (synthetic, 45° dipping precut). The dashed lines mark the precut; other symbols as in Fig. 3.

following the isotropic experiment (E1). These differences are analyzed in detail in the following sections (see summary of results in Table 1).

4.1. Upward propagation of new faults

The role of mechanical discontinuities on the propagation of fractures and faults represents one of the main problems faced by fracture mechanics and material science (see Gudmundsson, 2011, for a summary); as such, it has been the object of several studies. Numerical models, and particularly those based on boundary elements approaches (e.g., Cooke and Pollard, 1997; Roering et al., 1997; Cooke et al., 2000; d'Alessio and Martel, 2004; Cooke and Madden, 2014), yielded encouraging results for geological applications. Among other workers, Roering et al. (1997) analyzed the influence of horizontal, bedding-plane slip on the propagation of a newly-formed, blind reverse fault, suggesting: 1) an increased tendency of the new fault to propagate upward when the frictional plane is above it, and 2) a reduced tendency for the same new fault to propagate further when its tip reaches the pre-existing plane.

Although we investigate how pre-existing discontinuities affect the evolution of a normal fault, our experiments yield results qualitatively similar to those obtained by Roering et al. (1997); we observe different velocities in fault propagation, however, also depending on 1) the location of the upward-propagating fault and 2) the orientation of the pre-existing discontinuities (precuts). The upward propagation rate of our newly-formed faults is not constant over time (Fig. 10a), but it either accelerates or decelerates during all experiments. Below we first recall how these faults grow in the isotropic experiment, then analyze the fault-propagation rate in experiments with differently oriented precut.

4.1.1. The isotropic model

The main fractures that can be visually detected on the side of the clay layer in the Early Stage of the isotropic experiment (E1) formed with an acute angle with the vertical σ_1 (ca. 30°), the characteristic angle of shear fractures (Fig. 3a). Such shear fractures (Mode II) – i.e. the upward-propagating faults – connect to each other through small vertical fractures reminiscent of wing cracks (Mode I). In general, this propagation pattern is similar to that expected from crack models and it has been observed both in

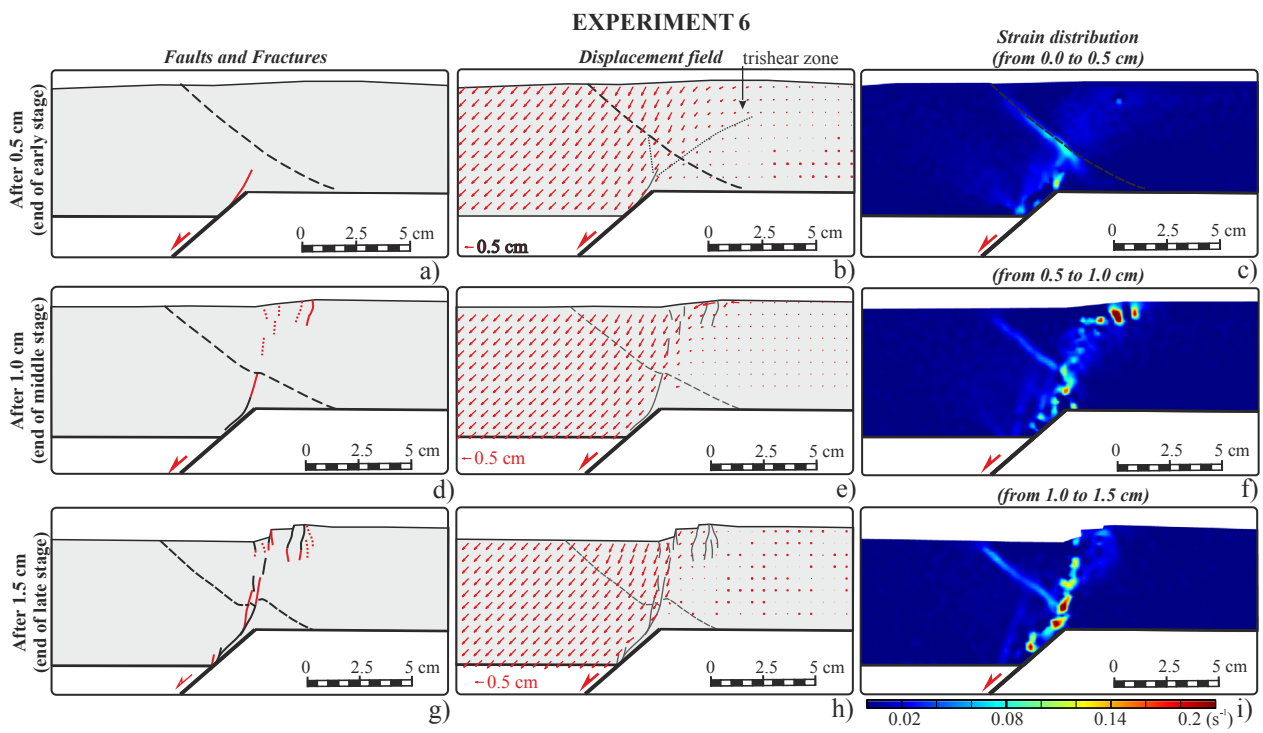

Fig. 8. Side view of E6 (antithetic, 45° dipping precut). The dashed lines mark the precut; other symbols as in Fig. 3.

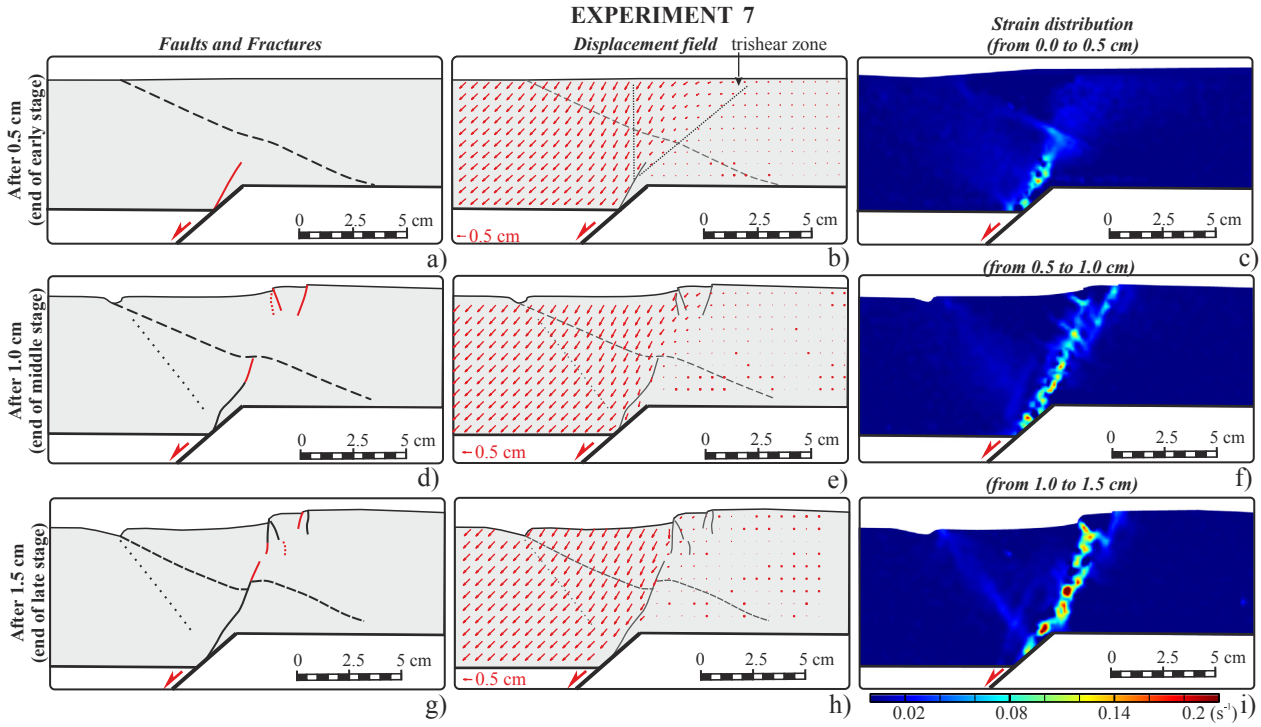

Fig. 9. Side view of E7 (antithetic, 30° dipping precut). The dashed lines mark the precut; other symbols as in Fig. 3.

laboratory tests on rock samples and in field studies (see Scholz, 2002 for a summary and references on this topic). The profile of upward propagation of these faults reflects this process (Fig. 10a).

At the very beginning of the experiment the stress concentration at the buried tip of the master fault (i.e. at the boundary between the rigid blocks) increases and generates small *en echelon* Mode I fractures, resulting in a low fault propagation rate (Fig. 10a). When the small, Mode I fractures connect to one another, and become visually detectable Mode II fractures, the propagation rate increases abruptly and the shear fractures develop up to 1.5 cm from the original location of the tip of the master fault. This process is followed by another phase of Mode I crack formation, and consequently the fault propagation slows down. During the Late Stage the upward-propagating fault connects through Mode I cracks located at its tip with downward-propagating faults, thereby increasing the extent of its upward propagation.

In summary, the upward propagation rate of newly-formed faults in the isotropic experiment is not constant; it is very slow during the formation of Mode I cracks, but increases abruptly when the cracks start connecting and forming shear fractures. This produces an asymmetric propagation profile, with a nucleation phase dominated by the formation of small cracks at the tip of the shear fractures and limited upward propagation, followed by a growing phase where small cracks connect to one another to form larger shear factures, thus determining faster upward propagation.

4.1.2. Fault-tip upward propagation below the precut

At the very beginning of all experiments with precut, the characteristics of the upward propagation of new faults are rather similar to those seen in the isotropic experiment (Fig. 10b). However, significant differences in the upward propagation rates start appearing later on, when the newly-formed, upward-propagating shear fractures extend beyond 1 cm distance from the base of the clay layer. At this point, in experiments where the precut is antithetic to the master fault the upward-propagation rate of newly-formed faults is slightly faster than in the isotropic case (Fig. 10b) but slower than in the experiment where the precut is horizontal. The upward-propagation rate of newly-formed faults becomes increasingly faster for an increase in the dip of the precut in experiments where the precut is synthetic to the master fault. Our results thus confirm that discontinuities located above a fault accelerate its upward propagation rate, but this tendency is controlled by the dip angle and dip direction of the precut. This occurrence is probably related to the stress intensity at the propagating tip of upward-propagating faults; as shown by the strain analysis in the various experiments, which is larger when slip on the discontinuity is larger.

4.1.3. Fault-tip upward propagation across the precut

A propagating fracture that meets a discontinuity may stop, be deflected, or penetrate such discontinuity. The works by Hutchinson (1996), Xu et al. (2003), and Wang and Xu (2006) established that the behavior of the propagating fracture strongly depends on the *toughness* of the encountered discontinuity, i.e. on the ability of a material containing a crack to resist fracturing. When the toughness is larger than the total strain energy, the propagating fracture penetrates the discontinuity. Conversely, when the toughness is lower than the total strain energy, the propagating fracture is deflected and joins the discontinuity.

In our experiments we observe that the precut orientation controls the propagation process of newly-formed faults when their tip approaches the precut itself. We also observe that a steeper precut dip angle, which determines an increased shear stress with respect to normal stress, favors slip along the precut. More slip is thus indicative of a relatively lower toughness of the discontinuity, and consequently it is also indicative of a promoted fracture deflection. The deflection of upward-propagating faults is promoted in experiments where the dip of the precut is >10° (E4, E5, E6, and E7; Fig. 10b). In experiments with antithetic precut, the sense of slip on the precut is opposite to that of the main, upward-

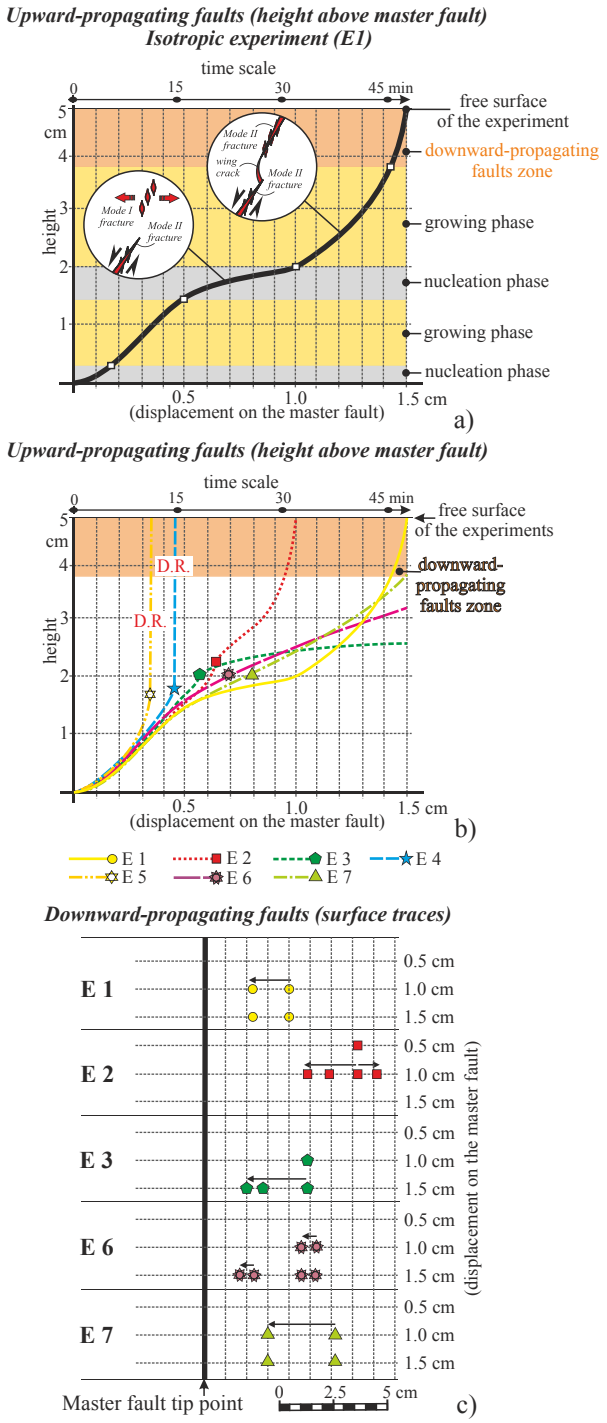

Fig. 10. **a**) Progression of upward propagation of newly-formed fault in the isotropic experiment; the color shaded area marks the various stages of propagation. **b**) Progression of upward propagation of newly-formed faults in all experiments. Point symbols mark the position of the precut. Notice that the lines describing the progression of E4 and E5 become vertical when the newly-formed faults join the pre-existing discontinuity and reactivate it (Discontinuity Reactivated; D.R.). The orange shaded area marks the zone of the clay layer where downward-propagating faults tend to develop. **c**) Position of the surface traces of downward-propagating faults in each experiment. E4 and E5 are not reported because no surficial faults were detected in these experiments. (For interpretation of the references to colour in this figure legend, the reader is referred to the web version of this article.)

propagating faults; hence, deflection is inhibited along such an unfavorably oriented plane, resulting in a delayed upward-propagation of newly-formed faults.

4.1.4. Fault-tip upward propagation above the precut

In E4 and E5 the newly-formed faults reactivate the precut and quickly reach the free surface. In E2 the upward-propagating fault accelerates after connecting with the horizontal precut. In all other experiments (E3, E6, and E7) the newly-formed faults decelerate their upward propagation as they extend beyond the precut (Fig. 10b). In these experiments, such deceleration is probably related to the slip on the precut that accommodates part of the shear strain.

4.2. Antithetic faults

Another important difference between the isotropic experiment (E1) and the experiments with precut (E2-7) concerns the formation of antithetic faults (Figs. 3–9). In the isotropic case, an antithetic fault evolves throughout the experiment and accommodates the material deformation in the hanging wall of the main synthetic upward-propagating faults (Fig. 3). It nucleated at the bend formed by the master fault on the rigid blocks and the newly-formed upward-propagating fault. The same is seen in E3 (Fig. 5), but in this case the antithetic faults are located at the bends of the synthetic upward-propagating fault and terminate their own propagation against the precut.

In E2 the antithetic faults cannot be visually detected (left panels in Fig. 4), though some strain concentrates where an antithetic fault may be expected to form (Fig. 4e), i.e. on the hanging wall side of the trishear zone. Such an occurrence can be explained by the smooth trajectory of the synthetic fault, which derives from the faster growth rate and lower hanging wall deformation than those seen in other experiments.

In E4 and E5 (Figs. 6 and 7) the synthetic precuts have a dip $\geq 30°$ and have been partially (E4) or totally reactivated (E5). The reactivation prevents the formation of new antithetic faults by accommodating most of the hanging wall deformation.

In E6, the precut is antithetic with respect to both the master fault and the newly-formed upward-propagating faults. In this case, the partial reactivation of the precut prevents the formation of new antithetic faults (Fig. 8). In E7, the antithetic precut only partially prevents the formation of antithetic structures because its reactivation occurs only in the very early stage of deformation (Fig. 9a). No antithetic faults are formed in later stages (Fig. 9f, i), although a strain concentration is seen along an alignment whose attitude and dip are compatible with those of an incipient antithetic fault plane.

4.3. Shallow brittle structures

During all experiments, the movement of the rigid blocks and the development of upward-propagating faults produce folding, that is to say, bending of the free surface: anticlines above the tip of the master fault and synclines over the rigid hanging wall. In most of our experiments we observe faults that form near the free surface and propagate downward, evolving through time and space during the different stages of the experiments, yet they are normally confined at very shallow depth. As already mentioned, these minor faults are related with the bending moment caused by the upward-propagation of the main newly-formed synthetic fault. Shallow downward-propagating structures form in five experiments: E1, E2, E3, E6, and E7. They are located along the anticline axis, i.e. where the tensile stress due to bending is largest. In contrast, downward-propagating faults do not form at all in E4 and

E5, likely because slip on the main synthetic fault reaches the free surface during the very early stages of deformation (Fig. 10b), thereby minimizing the bending moment at shallow depth. Hereafter, we adopt the vertical projection to the free surface of the tip of the master fault on the footwall rigid block as a reference for the position of these shallow faults (Fig. 10c); positive distance is toward the footwall.

At the free surface of the isotropic experiment (E1) the first structure nucleates near the anticline axis at a distance of 2.0 cm (Figs. 3, and 10c). The second surface fault forms at a shorter distance and links with the upward-propagating fault during the late stage of the experiment.

In E2, a shallow brittle structure forms since the Early Stage, likely because the development of the fold related with the upward-propagating fault is faster than in other experiments. This shallow fault is located farther away into the footwall than shallow faults observed in other experiments (Fig. 10c), yet it remains within the trishear zone. In the Middle Stage, other shallow faults quickly form at shorter distance but showing only little offset.

In E3 a shallow fault displaces the free surface at 2.5 cm distance in the Middle Stage (Figs. 4, and 10c). During the Late Stage most of the surface deformation concentrates on this fault because of the significant slowdown in the evolution of the upward-propagating but still blind faults, likely as a result of the interaction with the precut. This interaction causes a small change of the monocline shape, and, consequently, the maximum tensile stress is always located in the same portion of the fold. Minor faults located at shorter distance are related to the progression of the – minimal, yet clearly visible – fold.

In E6 (Fig. 8) and E7 (Fig. 9), the downward-propagating faults are well developed and offset significantly the free surface. This is due to the reactivation of the precut that tightens the anticline at shallow depth, thereby increasing the tensile stress on the fold extrados.

In all experiments, the downward-propagating faults form progressively from the footwall toward the hanging wall, though their initial position and vertical offset are variable (Fig. 10c). In the experiments where the upward-propagating faults reach the surface (E1 and E2) the innermost shallow faults form in the early stages and are then linked to the upward-propagating faults.

4.4. Shape of the free surface and migration of the syncline hinge

The shape of the anticlines and synclines and the position of their hinges control the development of secondary brittle structures. Such direct correlation was illustrated in Section 4.3 where we highlighted how the shape of the anticlines and the migration of their hinge points lead to the formation of secondary shallow faults – i.e. the bending-moment faults – while the master fault remains blind.

To analyze the warping of the free surface we construct a formline obtained by connecting the shallowest displacement vectors; this allows us to avoid including unwanted artifacts due to the unevenness of the top of the clay layer. All experiments show a different evolution of the fold shape and of the space-time migration of fold hinges (Fig. 11). To highlight the peculiarities of each experiment, we reconstruct 1) the cumulative and 2) the incremental shape changes (Fig. 11a and c, respectively) at the same intervals as in the fault analyses. The cumulative profiles provide a way of comparing our experimental results with the bedrock of a hypothetical sedimentary basin, i.e. with the shape of the basin floor. Conversely, since erosion, transport, and deposition processes respond dynamically to the changes of the accommodation space, the incremental profiles provide useful information on the evolution/architecture of a sedimentary infill. Similarly to the analysis of shallow faults (Section 4.3), we adopt the vertical projection to the free surface of the tip of the master fault on the footwall rigid block as a reference for the position of fold axes (Fig. 11b and d); in this case, however, positive distance is toward the hanging wall.

A comparison of the hanging wall of all experiments shows anticline limbs with different inclinations and a variable degree of openness of the synclines (Fig. 11).

4.4.1. Early stage (from 0 to 0.5 cm)

In the isotropic experiment (E1) the syncline hinge is at about 2.5 cm (Fig. 11a). In most of the other experiments, the syncline hinge is closer to the tip of the master fault, with the exception of E3 whose syncline hinge is the farthest (Fig. 11a). Such differences are due to the different propagation rates of the upward-propagating faults and/or to the amount of slip taken on by the precut. In E3, for instance, the position of the syncline hinge could be related to the slower development of the upward-propagating fault or to a weak reactivation of the precut or to both conditions. The syncline hinge of E2 is the closest, likely because of the faster growth rate of the upward-propagating fault. Regarding E4, E6, and E7, the syncline hinge stays nearly in the same position even if the fault evolution history and the resulting fold shape are different. Indeed in E4 the reactivation of the synthetic precut produces a very open anticline and syncline, whereas in E6 and E7 slip on the precut tightens the shape of the syncline without shifting its hinge (Fig. 11a, b). In E7 a small syncline also forms far away into the hanging wall in correspondence with the precut cutoff and likely due to the partial reactivation of the precut itself. Notice that in all experiments the subsidence of the syncline hinge is about 0.3 cm (Fig. 11a). In E5 no syncline develops because the early reactivation of the precut quickly transfers slip up to the free surface, hence drastically shortening the bending phase.

4.4.2. Middle stage (from 0.5 to 1.0 cm)

In the Middle Stage the differences between subsequent experiments increase, though all syncline hinges migrate toward the footwall. In E1, the syncline hinge migrates 0.29 cm vertically and 0.6 cm horizontally (Fig. 11b and d). E2, E3, and E4 show a similar trend. Conversely, E6 and E7 display significant lowering without any horizontal shift. This is likely due to the concurrent evolution of fold-related faulting and slip on sections of the precut (Figs. 8 and 9). This trend is more evident in E6 because the precut is more favorably oriented for being reactivated (dip = 45°). Downward-propagating faults begin to be well developed and offset the free surface. In E3 the anticline is also reshaped by a small graben-like structure. The precut reactivation in E4 increases the size of the hollow located on the hinge zone of the major anticline. In E2 the fast development of the upward-propagating fault produces a sort of box fold (Fig. 11a). The analysis of the surface deformation (Fig. 11c) highlights that this box fold is produced by a rapid migration of the syncline hinge due to the evolution of the upward-propagating fault. Fig. 11b and d show that E1, E2, and E3 have approximately the same horizontal shift values, but the vertical component in E1 and E3 is less pronounced than that of E2 and it is insufficient to produce a significant change in the shape of the syncline.

4.4.3. Late stage (from 1.0 to 1.5 cm)

In E1 the connection between upward- and downward-propagating faults concludes the blind phase of the system. The synclinal hinge migrates toward the footwall at an almost constant rate (Fig. 11b and d). In E3, the evolution of the upward-propagating fault is drastically slowed down by the precut (Fig. 10b). Such interaction enhances the little graben near the anticline hinge. In E4 the reactivation of the precut contrasts the migration of the

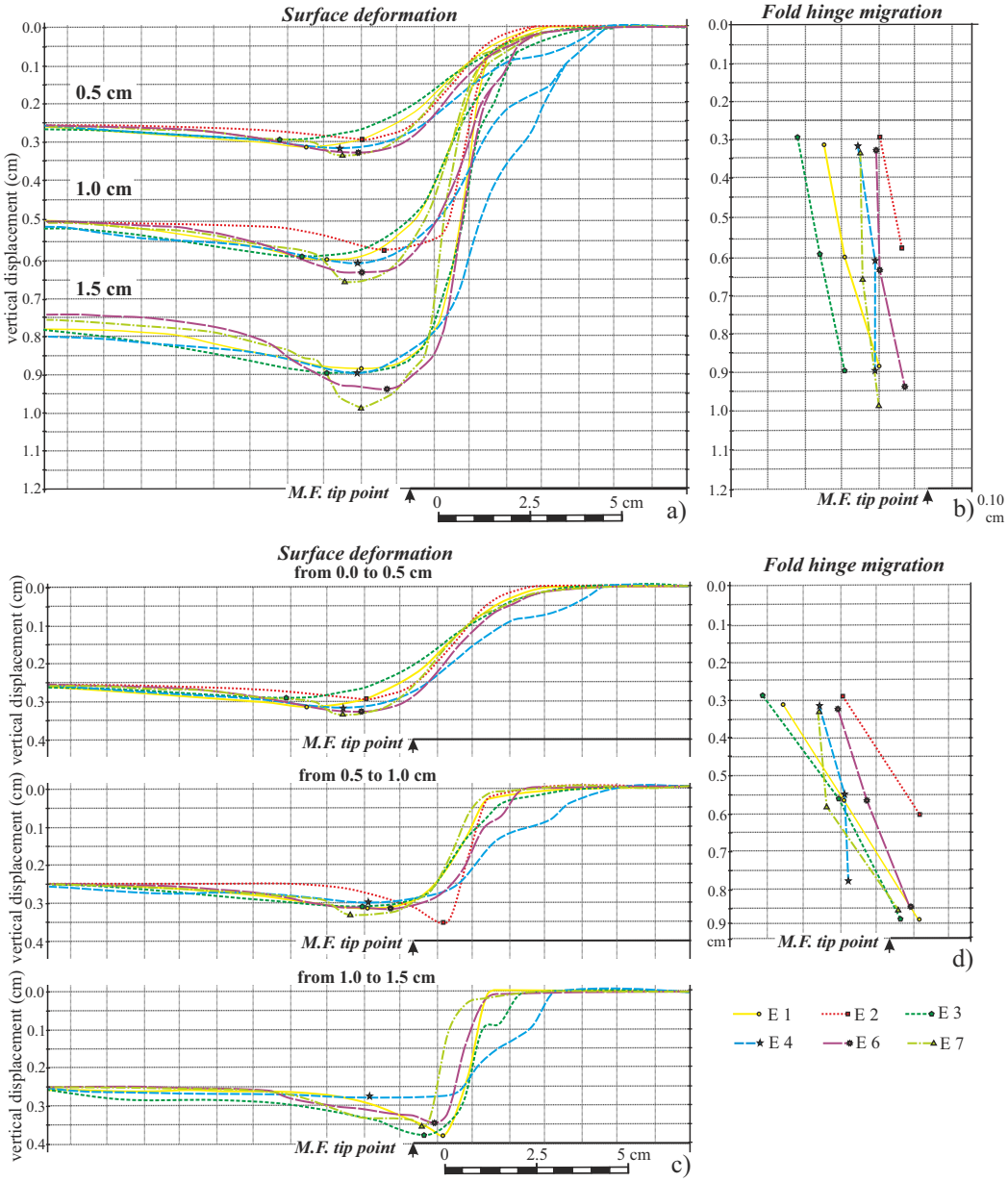

Fig. 11. Profiles of the cumulative (**a**) and incremental (**c**) surface deformation of all experiments, except for E5, after 0.5, 1.0 and 1.5 cm of total displacement on the master fault, and diagrams of the corresponding cumulative (**b**) and incremental (**d**) migration paths of the synclinal hinges. In all diagrams the point symbols mark the position of synclinal hinges taken as the lowest point on the profiles.

syncline hinge, resulting in its negligible horizontal shift (Fig. 11d). Fig. 11c shows how the slip on this anti-listric (convex up) fault results in a uniform subsidence of the hanging wall. In E6 and E7 the horizontal migration of the syncline hinge restarts only after that the downward-propagating faults are well developed and the upward-propagating faults cross the precut.

4.5. Modeling limitations

The geometry and kinematics of faults and folds that develop in an extensional system where variably oriented pre-existing discontinuities are located above a master normal fault can be successfully simulated using analog modeling. Before applying our results to analyze natural systems, however, it is important to consider some intrinsic limitations of our experiments.

Our experimental apparatus reproduces a planar, 45°-dipping master fault. In nature, extensional faults may have a listric geometry that induces hanging wall deformation driven by the sliding of rocks on a curved fault surface (e.g. rollover and drag folds), potentially broadening the newly-generated accommodation space (Resor and Pollard, 2012). Friction on the master fault plane and secondary normal- and reverse-drag folds or a combination thereof may also control hanging wall deformation (e.g., Schlische, 1995).

Other important limitations regard the frictional properties and the number of precuts within the clay layer. They may strongly affect the evolution of the extensional system, amplifying or reducing phenomena that we observe in our experiments (Roering et al., 1997). The shear strength of the precut also depends on its depth, because the deeper the precut, the higher the normal stress acting on it. Therefore, for any given precut setting, a shallower

precut can be reactivated more easily. A better characterization of precuts also improves the possibility of comparing them to natural discontinuities.

In nature, the dip of the master fault strongly affects both the associated folds and any secondary brittle structures (Withjack et al., 1990). When the master fault is steeper the associated fold is tighter and determines an early development of bending-moment faults. Conversely, when the master fault dip is gentler, the associated fold is open and the extensional structures – or downward-propagating faults – may not form at all because the curvature radius is larger. Moreover, the normal faults may rotate during the evolution (domino rotation), changing their dip and affecting the shape of the accommodation space.

The usage of rigid hanging wall and footwall blocks is yet another simplification. In the case of seismogenic faults, for instance, surface deformation is not only produced by coseismic elastic dislocation but also by postseismic relaxation. This is related with the viscous roots and the viscoelastic properties of the lower crust and upper mantle that may contribute to the surface deformation by increasing the wavelength of the surface displacement (Wang et al., 2006; Bürgmann and Dresen, 2008).

4.6. Natural extensional systems

Several currently active extensional systems are located in continental regions that were affected by contractional processes in earlier tectonic phases. These tectonic systems may exhibit various degrees of structural maturity depending on the age of inception and on the strain rate of the ongoing extension.

In a very early stage, the extension of an orogenic belt is mainly, though not exclusively, testified by earthquake focal mechanisms and geodetic strain. For instance, the Pyrenees is a mountain chain where the landscape is still dominated by geomorphic features generated in a contractional setting, but where the analysis of focal mechanisms demonstrates that current deformation is dominantly extensional (Chevrot et al., 2011; Lacan and Ortuño, 2012). Considering the tectonic setting of the region and, specifically, the double vergence of the chain, one could speculate that in the Pyrenees some interactions between older contractional structures and younger extensional faults might be occurring in a framework similar to either E4-5 or E6-7.

Such interactions have been extensively documented also in the Apennines, where recent earthquakes shed light on the direct interaction between youthful extensional faults and inherited thrusts that affect both their development and their surface signature. For example, Miocene thrusts appear to control the extent of 40°-dipping normal faults that were responsible for the M_w 6.0 and 5.7 mainshocks of the September 1997, Colfiorito, earthquake sequence (Chiaraluce et al., 2003). In the case of the April 2009, L'Aquila earthquake sequence the first mainshock (6 April, M_w 6.3) was caused by slip on a 40–50°-dipping normal fault; this master fault branches upward at 3–5 km depth where it intersect a Miocene thrust dipping 10° in the same dip direction as the master fault and creates bending-moment faulting at the ground surface (Bonini et al., 2014). In the second mainshock (7 April, M_w 5.4), that was caused by another 40–50°-dipping normal fault with an upper limit at about 5 km depth, just below a 20–30°-dipping Miocene thrust; as a result, it showed no connection with the normal faults lying above it, especially well imaged by seismic reflection lines (Bigi et al., 2013). Altogether these examples recalls the early-middle stages of E3 and E4 and, considering cases analyzed by Valensise and Pantosti (2001), suggest that other large active normal faults in the Apennines may be developing in a framework similar to any other of our experiments.

In summary, although extension is currently the dominating tectonic mechanism both in the Pyrenees and in the Apennines, the structural architecture of these orogens reflects the activity of the large seismogenic normal faults only to a very limited extent. Instead, their landscape and their earthquake potential are clearly dominated by the interaction with inherited contractional structures, which ultimately affect the length, the width and the top depth of the active normal faults.

Another example of such interactions has been documented in the northern part of the Taiwan orogen that is affected by late Quaternary extension (e.g. Suppe, 1984; Teng, 1996; Hu et al., 2002). An active normal fault (Shanchiao Fault) located in the Taipei basin shows a ramp-flat-ramp geometry whose deeper ramp (dipping 60°) is an ancient extensional fault inherited from a pre-contractional phase (rifting phase of the Chinese Continental Margin). Its flat portion (dipping 15°) is a Neogene thrust fault, whereas the shallower ramp is a late Quaternary – hence newly-formed – normal fault (Chen et al., 2014). It is plausible that Quaternary extension reactivated the ancient extensional fault at depth, which propagated upward exploiting a segment of the low–angle inherited thrust and then reached the ground surface forming a new high-angle, normal fault. This unusual case of Quaternary fault development is reminiscent of the results of E3 and E4, and shows that also a 60°-dipping extensional fault, i.e. a fault steeper than the master faults in our experiments, may stop its upward propagation against an inherited low-angle structure.

Conversely, in a mature system the extensional faults are expected to be well developed and expressed at the surface. The Basin and Range Province is a renowned example of such a mature extensional system. However, also in this region extensional structures overprint older contractional structures (e.g. Wernicke, 1992; Parsons, 1995; Axen, 2007). Studies on major earthquakes of this area (e.g. the M_w 7.3, 1959, Hebgen Lake, Montana, and the M_w 6.9, 1983, Borah Peak, Idaho) demonstrate that the normal faults exposed at the surface are the direct expression of large, planar faults dipping 40°–70° and extending down to 12–16 km depth (Barrientos et al., 1987; Doser, 1989). Notice, however, that some of these fault planes coincide at depth with pre-existing contractional structures (thrust faults) reactivated as normal faults during the extensional phase (Doser, 1989; West, 1992) in a way very similar to what can be observed in E4 and E5. The existence of youthful faults confined at depth (blind faults) and interacting with inherited thrusts that are unfavorably oriented with respect to the current stress field was described in great detail by West (1989, 1992), testifying that inherited structures may play an active role even in regions that exhibit a hypermature stage of development.

In summary, depending on the local configuration or on the degree of structural maturity, the inherited structures may directly affect the evolution of youthful extensional faults. Our experiments may help characterizing the evolutionary stage of these faults and understand the causal relationships between the master fault at depth and other structural and geomorphic features.

5. Conclusions

We investigated how pre-existing discontinuities affect the growth of extensional structures connected to the displacement on an initially-blind master normal fault. To this end, we used analog models that take advantage of an innovative technique for performing a precut into a clay (wet kaolin) layer laid on top of a master fault, simulated by the sliding of two rigid blocks. Using this original setup, we carried out six experiments in which the precut has various orientations with respect to the master fault, and compared them to another experiment without any precut

(isotropic). All other conditions were identical for all seven experiments.

Our results show that the presence of a precut can either accelerate or decelerate the upward propagation of the master fault and exert control on several other factors summarized below and in Table 1;

- a horizontal precut promotes the tendency to grow of upward-propagating faults;
- low-angle synthetic precuts (e.g. dip 10°) slow down the propagation of upward-propagating faults, but also promote the formation and evolution of shallow downward-propagating surface faults associated with bending moment;
- high-angle precuts (dip>30°) are prone to be reactivated and may serve as a preferential way for the master fault to quickly transfer slip up to the free surface. If the dip of the precut is lower than that of the master fault, the new fault system will show an antilistric geometry;
- when the precut is antithetic with respect to the master fault one may expect an increase of the growth of the upward-propagating faults and a reactivation of the precut as antithetic faults;
- the various interactions between the growing master fault and the precut also affect the shape of the fault-related syncline–anticline pair and, in turn, the shape of the resulting accommodation space.

These findings may improve our understanding of how extensional fault systems evolve in presence of structures inherited from previous tectonic phases, such as the normal faults that currently affect older orogenic belts. We also suggest that the analysis of the shape and architecture of fault-related continental basins carried out in the light of our findings may provide useful constraints for reconstructing the actual geometry of the master fault at depth.

Acknowledgments

All experiments were carried out at the 3D Modelling Laboratory at University of Pavia (www.3dmodellinglaboratory.it). The work was supported by the INGV Project “Abruzzo” (code: RBAP10ZC8K_003), funded by the Italian Ministry for Education, University and Research (MIUR). The authors thank the editor C.W. Passchier, an anonymous reviewer and E. Tavarnelli for thoughtful reviews of the manuscript that greatly improved the paper.

References

Ahmad, M.I., Dubey, A.K., Toscani, G., Bonini, L., Seno, S., 2014. Kinematic evolution of thrust wedge and erratic line length balancing: insights from deformed sandbox models. Int. J. Earth Sci. 103 (1), 329–347. http://dx.doi.org/10.1007/s00531-013-0947-8.

Axen, G., 2007. Research focus: significance of large-displacement, low-angle normal faults. Geology 35, 287–288. http://dx.doi.org/10.1130/0091-7613(2007)35[287:RFSOLL]2.0.CO;2.

Allmendinger, R.W., 1998. Inverse and forward numerical modeling of trishear fault-propagation folds. Tectonics 17, 640–656. http://dx.doi.org/10.1029/98TC01907.

Barrientos, S.E., Stein, R.S., Ward, S.N., 1987. Comparison of the 1959 Hebgen Lake, Montana and the 1983 Borah Peak, Idaho, earthquakes from geodetic observations. Bull. Seismol. Soc. Am. 77, 784–808.

Bigi, S., Casero, P., Chiarabba, C., Di Bucci, D., 2013. Contrasting surface active faults and deep seismogenic sources unveiled by the 2009 L'aquila earthquake sequence (Italy). Terra Nova 25, 21–29.

Bonini, L., Dallagiovanna, G., Seno, S., 2010. The role of pre-existing faults in the structural evolution of thrust systems: insights from Ligurian Alps (Italy). Tectonophysics 480, 73–87. http://dx.doi.org/10.1016/j.tecto.2009.09.021.

Bonini, L., Di Bucci, D., Toscani, G., Seno, S., Valensise, G., 2011. Reconciling deep seismogenic and shallow active faults through analogue modelling: the case of Messina straits (southern Italy). J. Geol. Soc. 168 (1), 191–199. http://dx.doi.org/10.1144/0016-76492010-055.

Bonini, L., Di Bucci, D., Toscani, G., Seno, S., Valensise, G., 2014. On the complexity of surface ruptures during normal faulting earthquakes: excerpts from the 6 April 2009 L'Aquila (central Italy) earthquake (Mw 6.3). Solid Earth 5, 389–408. http://dx.doi.org/10.5194/se-5-389-2014.

Bürgmann, R., Dresen, G., 2008. Rheology of the lower crust and upper mantle: evidence from rocks mechanics, geodesy, and field observations. Annu. Rev. Earth Planet. Sci. 36, 531–557. http://dx.doi.org/10.1146/annurev.earth.36.031207.124326.

Chen, C.-T., Lee, J.-C., Chan, Y.-C., Lu, C.-Y., Teng, L.S.-Y., 2014. Elucidating the geometry of the active Shanchiao Fault in the Taipei metropolis, northern Taiwan, and the reactivation relationship with pre-existing orogen structures. Tectonics. http://dx.doi.org/10.1002/2013TC003502.

Chevrot, S., Sylvander, M., Delouis, B., 2011. A preliminary catalog of moment tensors for the Pyrenees. Tectonophysics 510, 239–251.

Chiaraluce, L., Ellsworth, W.L., Chiarabba, C., Cocco, M., 2003. Imaging the complexity of an active normal fault system: the 1997 Colfiorito (central Italy) case study. J. Geophys. Res. 108 (B6), 2294. http://dx.doi.org/10.1029/2002JB002166.

Cloos, E., 1968. Experimental analysis of Gulf Coast fracture patterns. AAPG Bull. 52, 420–444.

Collettini, C., Sibson, R.H., 2001. Normal faults, normal friction? Geology 29 (10), 927–930. http://dx.doi.org/10.1130/0091-7613.

Cooke, M.L., Mollema, P., Pollard, D.D., Aydin, A., 2000. Interlayer slip and fracture clusters within East Kaibab monocline: numerical analysis and field investigations. In: Cosgrove, J., Ameen, M. (Eds.), Geological Society of London Special Publication – Drape Folds and Associated Fractures, vol. 169, pp. 23–49.

Cooke, M.L., Madden, H.M., 2014. Is the earth lazy? A review of work minimization in fault evolution. J. Struct. Geol. 66, 334–346.

Cooke, M.L., Schottenfeld, M.T., Buchanan, S.W., 2013. Evolution of fault efficiency at restraining bends within wet kaolin analog experiments. J. Struct. Geol. 51, 180–192.

Cooke, M.L., Pollard, D.D., 1997. Bedding-plane slip in initial stages of fault-related folding. J. Struct. Geol. 19 (3), 567–581.

Cooke, M.L., van der Elst, N.J., 2012. Rheologic testing of wet kaolin reveals frictional and bi-viscous behavior typical of crustal materials. Geophys. Res. Lett. 39. http://dx.doi.org/10.1029/2011GL050186.

Cosgrove, J.W., Ameen, M.S., 2000. A comparison of the geometry, spatial organization and fracture patterns associated with forced folds and buckle folds. In: Cosgrove, J., Ameen, M. (Eds.), Geological Society of London Special Publication – Drape Folds and Associated Fractures, vol. 169, pp. 7–21.

d'Alessio, M.A., Martel, S.J., 2004. Fault terminations and barriers to the fault growth. J. Struct. Geol. 26, 1885–1896.

Dalmayrac, B., Molnar, P., 1981. Parallel thrust and normal faulting in Peru and constraints on the state of stress. Earth Planet. Sci. Lett. 55, 473–481.

Davis, D., Suppe, J., Dahlen, F.A., 1983. Mechanics of fold-and-thrust belts and accretionary wedges. J. Geophys. Res. 88 (B2), 1153–1172.

Di Domenica, A., Bonini, L., Calamita, F., Toscani, G., Galuppo, C., Seno, S., 2014. Analogue modeling of positive inversion tectonics along differently oriented prethrustingnormal faults: an application to the Central-Northern Apennines of Italy. Bull. Geol. Soc. Am. 126 (7–8), 943–955. http://dx.doi.org/10.1130/B31001.1.

Doser, D.I., 1989. Source parameters of Montana earthquakes (1925–1964) and tectonic deformation in the northern intermountain seismic Belt. Bull. Seismol. Soc. Am. 79, 31–50.

Eisenstadt, G., Sims, D., 2005. Evaluating sand and clay models; do rheological differences matter? J. Struct. Geol. 27, 1399–1412, 2005.

Elter, P., Giglia, G., Tongiorgi, M., Trevisan, L., 1975. Tensional and compressional areas in the recent (Tortonian to present) evolution of the Northern Apennines. Boll. Geofis. Teor. Appl. 42, 3–18.

Faccenna, C., Nalpas, T., Brun, J.P., Davy, P., Bosi, V., 1995. The influence of pre-existing faults on normal fault geometry in nature and in experiments. J. Struct. Geol. 17, 1139–1149.

Galuppo, C., Toscani, G., Turrini, C., Bonini, L., Seno, S., 2015. Fracture patterns evolution in sandbox fault-related anticlines. Italian J. Geosci. http://dx.doi.org/10.3301/IJG.2014.39.

Garcia, D., 2011. A fast all-in-one method for automated post-processing of PIV data. Exp. Fluids 50, 1247–1259. Springer-Verlag.

Gudmundsson, A., 2011. Rock Fractures in Geological Processes. Cambridge University Press.

Hardy, S., Ford, M., 1997. Numerical modelling of trishear fault-propagation folding and associated growth strata. Tectonics 16 (5), 841–854.

Hu, J.-C., Yu, S.-B., Chu, H.-T., Angelier, J., 2002. Transition tectonics of northern Taiwan induced by convergence and trench retreat. Geol. Soc. Am. Special Pap. 358, 149–162.

Hubbert, M.K., 1937. Theory of scale models as applied to the study of geologic structures. Geol. Soc. Am. Bull. 48, 1459–1520.

Hutchinson, J.W., 1996. Stresses and Failure Modes in Thin Films and Multilayers. Notes for a DCAMM Course. Technical University of Denmark, Lyngby, pp. 1–45.

Hyppolite, J.-C., Angelier, J., Roure, F., 1994. A major geodynamic change revealed by quaternary stress patterns in the Southern Apennines (Italy). Tectonophysics 230, 199–210.

Jackson, J.A., White, N.J., 1989. Normal faulting in upper continental crust: observations from regions of active extension. J. Struct. Geol. 11, 15–36.

Lacan, P., Ortuño, M., 2012. Active Tectonics of the Pyrenees: a review. J. Iber. Geol. 38 (1), 9–30.

Maino, M., Decarlis, A., Felletti, F., Seno, S., 2013. Tectono-sedimentary evolution of the Tertiary Piedmont Basin (NW Italy) within the Oligo-Miocene central Mediterranean geodynamics. Tectonics 32 (3), 593–619. http://dx.doi.org/10.1002/tect.20047.
Malavieille, J., 1993. Late orogenic extension in mountain belts: insights from the Basin and Range and the Late Paleozoic Variscan Belt. Tectonics 12 (5), 1115–1130.
Mandl, G., 2000. Faulting in Brittle Rocks: an Introduction to the Mechanics of Tectonic Faults. Springer-Verlag Berlin, Heidelberg New York.
Martel, S.J., Pollard, D.D., Segall, P., 1988. Development of simple fault zones in granitic rock, Mount Abbot quadrangle, Sierra Nevada, California. Geol. Soc. Am. Bull. 100, 1451–1465.
McClay, K., Bonora, M., 2001. Analog models of restraining stepovers in strike-slip fault systems. AAPG Bull. 85 (2), 233–260.
Miller, J.F., Mitra, S., 2011. Deformation and secondary faulting associated with basement-involved compressional and extensional structures. AAPG Bull. 95 (4), 675–689.
Molnar, P., England, P., Martinod, J., 1993. Mantle dynamics, uplift of the Tibetan plateau, and the Indian monsoon. Rev. Geophys. 31, 357–396.
Pan, B., Qian, K., Xie, H., Asundi, A., 2009. Two-dimensional digital image correlation for in-plane displacement and strain measurement: a review. Meas. Sci. Technol. 20 http://dx.doi.org/10.1088/0957-0233/20/6/062001.
Parsons, T., 1995. The basin and range province. In: Olsen, K. (Ed.), Continental Rifts: Evolution, Structure and Tectonics. Elsevier, Amsterdam, ISBN 044489-566-3, pp. 277–324. Accessed 25 September 2014 from United States Geological Survey web site. https://profile.usgs.gov/myscience/upload_folder/ci2012Jun2518224342680BRP_review_opt.pdf.
Paul, D., Mitra, S., 2013. Experimental models of transfer zones in rift systems. AAPG Bull. 97 (5), 759–780.
Philippon, M., Willinghofer, E., Sokoutis, D., Corti, G., Sani, F., Bonini, M., Cloetingh, S., 2015. Slip re-orientation in oblique rifts. Geology 43, 147–150.
Pollard, D., Aydin, A., 1988. Progress in understanding jointing over the past century. Geol. Soc. Am. Bull. 100, 1181–1204.
Resor, P.G., Pollard, D.D., 2012. Reverse drag revisited: why footwall deformation may be the key to inferring listric fault geometry. J. Struct. Geol. 41, 98–109.
Roche, V., Homberg, C., Rocher, M., 2013. Fault nucleation, restriction, and aspect ratio in layered sections: quantification of the strength and stiffness roles using numerical modeling. J. Geophys. Res. 188, 4446–4460. http://dx.doi.org/10.1002/jgrb.50279.
Roering, J.J., Cooke, M.L., Pollard, D.D., 1997. Why blind thrust faults do not propagate to the Earth's surface: numerical modeling of coseismic deformation associated with thrust-related anticlines. J. Struct. Geol. 102, 901–912.
Schlische, R., 1995. Geometry and origin of fault-related folds in extensional settings. AAPG Bull. 79 (11), 1661–1678.
Scholz, C.H., 2002. The Mechanics of Earthquakes and Faulting, second ed. Cambridge University Press, New York, p. 471.
Segall, P., Pollard, D.D., 1983. Nucleation and growth of strike slip faults in granite. J. Geophys. Res. 88, 555–568.
Selverstone, J., 1988. Evidence for east–west crustal extension in the Eastern Alps: implications for the unroofing history of the Tauern Window. Tectonics 7, 87–105.
Suppe, J., 1984. Kinematics of arc-continent collision, flipping of subduction and back-arc spreading near Taiwan. Mem. Geol. Soc. China 6, 21–33.
Tavarnelli, E., 1996a. Ancient synsedimentary structural control on thrust ramp development: examples from the Northern Apennines, Italy. Terra Nova 8, 65–74.
Tavarnelli, E., 1996b. The effects of pre-existing normal faults on thrust ramp development: an example from the Northern Apennines, Italy. Int. J. Earth Sci. 85, 363–371.
Tavarnelli, E., Decandia, F.A., Renda, P., Tramutoli, M., Gueguen, E., Alberti, M., 2001. Repeated reactivation in the Apennine-Maghrebide system, Italy: a possible example of fault-zone weakening? In: Holdsworth, R.E., Strachan, R.A., Maglouglin, J.F., Knipe, R.J. (Eds.), Geological Society of London Special Publication 186, "The Nature and Tectonic Significance of Fault Zone Weakening, pp. 273–286.
Tavarnelli, E., Renda, P., Pasqui, V., Tramutoli, M., 2003. The effects of post-orogenic extension on different scales: an example from the Apennine-Maghrebide fold-and-thrust belt, SW Sicily. Terra Nova 15, 1–7.
Teng, L.S., 1996. Extensional collapse of the northern Taiwan mountain belt. Geology 24 (10), 949–952.
Thielicke, W., 2014. The Flapping Flight of Birds – Analysis and Application. Phd thesis. Rijksuniversiteit, Groningen.
Thielicke, W., Stamhuis, E.J., 2014. PIVlab – Time-resolved Digital Particle Image Velocimetry Tool for MATLAB Version: 1.35. http://dx.doi.org/10.6084/m9.figshare.1092508.
Tong, H., Koyi, H., Huang, S., Zhao, H., 2014. The effect of multiple pre-existing weaknesses on formation and evolution of faults in extended sandbox models. Tectonophysics 626, 197–212.
Toscani, G., Bonini, L., Ahmad, M.I., Di Bucci, D., Di Giulio, A., Seno, S., Galuppo, C., 2014. Opposite verging chians sharing the same foreland: kinematics and interaction through analogue models (Central Po Plain, Italy). Tectonophysics 633, 268–282. http://dx.doi.org/10.1016/j.tecto.2014.07.019.
Tvedt, A.B.M., Rotevatn, A., Jackson, A.-L., Fossen, H., Gawthorp, R.L., 2013. Growth of normal faults in multilayer sequences: a 3D seismic case study from the Egersund Basin, Norwegian North Sea. J. Struct. Geol. 55, 1–20.
Valensise, G., Pantosti, D., 2001. The investigation of potential earthquake sources in peninsular Italy: a review. J. Seismol. 5, 287–306.
van Gent, H.W., Holland, M., Urai, J.L., Loosveld, R., 2010. Evolution of fault zones in carbonates with mechanical stratigraphy – insights from scale models using layered cohesive powder. J. Struct. Geol. 32, 1375–1391.
Wang, P., Xu, L.R., 2006. Dynamic interfacial debonding initiation induced by incident crack. Int. J. Solids Struct. 43, 6535–6550.
Wang, R., Lorenzo-Martìn, F., Roth, F., 2006. PSGRN/PSCMP-a new code for calculating co- and post-seismic deformation, geoid and gravity changes based on the viscoelastic-gravitational dislocation theory. Comput. Geosci. 32, 527–541. http://dx.doi.org/10.1016/j.cageo.2005.08.006.
Williams, G.D., Powell, C.M., Cooper, M.A., 1989. Geometry and kinematics of inversion tectonics. In: Cooper, M.A., Williams, G.D. (Eds.), Inversion Tectonics, Spec. Publ.. Geol. Soc, vol. 44, pp. 3–15.
Wernicke, B., 1981. Low-angle normal faults in the Basin and range province: nappe tectonics in an extending orogen. Nature 291, 645–648.
Wernicke, B., 1992. Cenozoic extensional tectonics of the U. S. Cordillera. In: Burchfiel, B.C., Lipman, P.W., Zoback, M.L. (Eds.), The Cordilleran Orogen; Conterminous U. S. The Geology of North America, vol. G-3. Geol. Soc. Am., Boulder, CO, pp. 553–581.
West, M.W., 1992. An integrated model for seismogenesis in the intermountain seismic belt. Bull. Seismol. Soc. Am. 82 (3), 1350–1372.
West, M.W., 1989. Neotectonics of the Darby-Hogsback and Absaroka Thrust Plates, Uinta County, Wyoming and Summit County, Utah with Applications to Earthquake Hazard Assessment. Ph.D. Thesis. Colorado School of Mines, Golden, CO.
Withjack, M.O., Callaway, S., 2000. Active normal faulting beneath a salt layer: an experimental study of deformation patterns in the cover sequence. AAPG Bull. 84 (5), 627–651.
Withjack, M.O., Jamison, W.R., 1986. Deformation produced by oblique rifting. Tectonophysics 126, 99–124.
Withjack, M.O., Oloson, J., Peterson, E., 1990. Experimental models of extensional forced folds. AAPG Bull. 74, 1038–1054.
Xu, L.R., Huang, Y.Y., Rosakis, A.J., 2003. Dynamic crack detection and penetration at interfaces in homogeneous materials: experimental studies and model predictions. J. Mech. Phys. Solids 51, 461–486.